ADVANCED FUNCTIONAL MATERIALS
www.afm-journal.de

High-Tensile Strength, Composite Bijels through Microfluidic Twisting

*Shankar P. Kharal, Robert P. Hesketh, and Martin F. Haase**

Rope making is a millennia old technique to collectively assemble numerous weak filaments into flexible and high tensile strength bundles. However, delicate soft matter fibers lack the robustness to be twisted into bundles by means of mechanical rope making tools. Here, weak microfibers with tensile strengths of a few kilopascals are combined into ropes via microfluidic twisting. This is demonstrated for recently introduced fibers made of bicontinuous interfacially jammed emulsion gels (bijels). Bijels show promising applications in use as membranes, microreactors, energy and healthcare materials, but their low tensile strength make reinforcement strategies imperative. Hydrodynamic twisting allows to produce continuous bijel fiber bundles of controllable architecture. Modelling the fluid flow field reveals the bundle geometry dependence on a subtle force balance composed of rotational and translational shear stresses. Moreover, combining multiple bijel fibers of different compositions enables the introduction of polymeric support fibers to raise the tensile strength to tens of megapascals, while simultaneously preserving the liquid like properties of the bijel fibers for transport applications. Hydrodynamic twisting shows potentials to enable the combination of a wide range of materials resulting in composites with features greater than the sum of their parts.

1. Introduction

Helices are ubiquitous structures in nature and technology. Their significance lies in their space saving configuration with importance both for macroscopic objects such as compact helical staircases, and for molecules such as the double helix of DNA with high genetic information density. While molecular or colloidal helices can be assembled by entropy,[1,2] molecular chirality,[3–5] DNA origami and vapor deposition techniques,[6,7] helices made of larger fibers can be obtained for example via the liquid rope coiling effect.[8,9]

Forming higher order helices or bundles with multiple fibers combines the properties of the individual fibers collectively. As a result, textile bundles show high tensile strength as well as high bending flexibility.[10] Traditionally, ropes are fabricated by attaching the ends of multiple filaments to rotating tools, which twist these around each other.[11] This millennia old technique continuous to be applied for the bundling of electrospun nanofibers into microropes.[12] Simultaneous nanofiber extrusion and bundling has been realized by either rotating fiber collection substrates, or rotating fiber extrusion nozzles.[13,14] However, bundle collection follows a batch protocol with limitations on the final bundle length. Moreover, the techniques are not applicable to delicate fiber materials that break easily upon mechanical load.

Here, we introduce an in situ technique to continuously twist fibers into bundles in a single step fashion. Our technique relies on applying well defined hydrodynamic shear stresses and can be applied to combine fibers with different material properties. To illustrate this principle, we show that twisting delicate soft matter fibers around a central support fiber results in high-tensile strength composite bundles.

We demonstrate hydrodynamic twisting for the bundling of fibers made of bicontinuous interfacially jammed emulsion gels (bijels)[15–17] formed by Solvent Transfer Induced Phase Separation (STrIPS).[18,19] Bijels are a class of materials with potential applications as catalytic microreactors,[20–22] energy storage materials,[23,24] separation membranes,[25] tissue engineering scaffolds,[26] and food products.[27] However, their low mechanical strength currently limits their wide application potentials.[28,25] Twisting bijel fibers into bundles introduces a versatile reinforcement strategy with manifold potentials. We analyze the hydrodynamic stresses during twisting and discover a subtle balance between axial and rotational forces. Controlling these allows for the formation of microropes with adjustable geometry.

2. Results

To obtain bijel fiber helices, a coaxial extrusion device is employed (**Figure 1**a). The device is composed of four glass capillaries

S. P. Kharal, Prof. R. P. Hesketh, Dr. M. F. Haase
Department of Chemical Engineering
Rowan University
Glassboro, NJ 08028, USA
E-mail: m.f.haase@uu.nl
Dr. M. F. Haase
Van't Hoff Laboratory of Physical and Colloid Chemistry
Department of Chemistry
Debye Institute of Nanomaterials Science
Utrecht University
Utrecht CH 3583, The Netherlands
The ORCID identification number(s) for the author(s) of this article can be found under https://doi.org/10.1002/adfm.202003555.

DOI: 10.1002/adfm.202003555

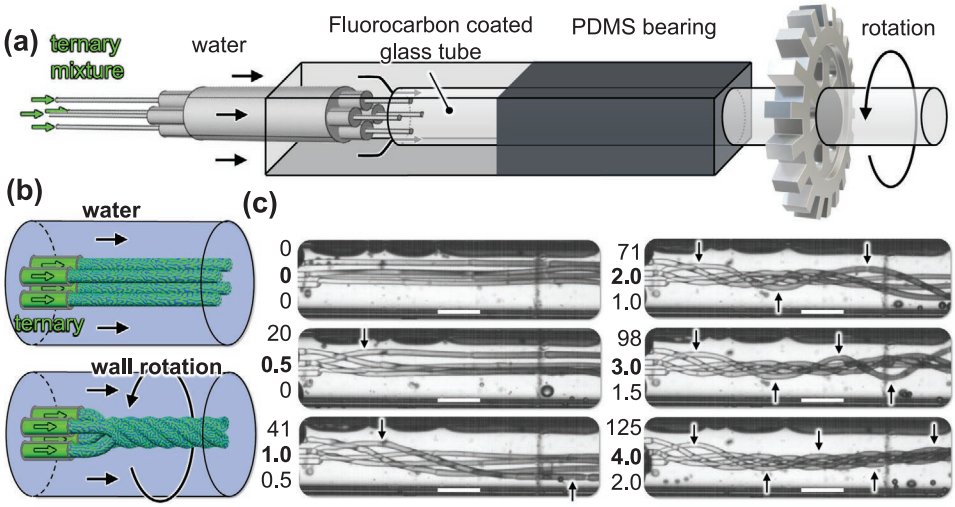

Figure 1. Principle of in situ hydrodynamic twisting. a) Schematics of the microfluidic device. A combination of capillaries with square and round cross-sections and different sizes are interdigitated and sealed with glue. A gear is connected to the rightmost capillary to allow for rotation. b) Schematics of bijel fiber helix formation upon activating the rotation of the outer channel wall. c) Micrograph time series of helix formation upon initiation of the wall rotation at 1900 rpm for a water flow rate of 1 mL min^{-1}. Each micrograph has three numbers on the left, representing (top to bottom) i) time in milliseconds, ii) number of wall rotations, iii) number of fibers twisted around the central axis. The arrows indicate half period (upward arrow) and full period (downward arrow) of the twisting for one selected fiber. All scale bars are 0.5 mm.

centered in a larger outer capillary (see the Supporting Information for detailed schematics of microfluidic device). Water is pumped through the outer capillary by means of a syringe pump. Four parallel fibers are obtained by flowing a ternary liquid mixture composed of oil (diethylphthalate or ethylene glycol dimethacrylate), ethanol, water, silica nanoparticles and cetyltrimethylammonium bromide (CTAB) under a pressure of 400 kPa through the four glass capillaries into the water stream.

Upon contacting the water stream, the ternary liquid mixture rapidly turns into a viscoelastic fiber, a process termed Solvent Transfer Induced Phase Separation (STrIPS).[18] In brief, ethanol diffuses from the ternary liquid mixture into the surrounding water. The rapid loss of ethanol causes water and diethylphthalate (DEP) to phase separate.

During STrIPS, CTAB modified nanoparticles accumulate on the interface between DEP and water, rigidifying the interface by jamming. The resulting structure is named bicontinuous interfacially jammed emulsion gel (short bijel).[15] The bijel is composed of a bicontinuous oil/water channel network and stabilized by a percolating film of nanoparticles.[16,17]

Bijel fibers are twisted into a helix by rotating the larger capillary around its own axis via a DC motor (Figure 1b). The rotating capillary is mounted in a polydimethoxysilane (PDMS) bearing to facilitate leak proof operation. Smooth rotation in the PDMS bearing is possible because of the lubrication provided by a coating of tridecafluoro-2-(tridecafluorohexyl)decyl trichlorosilane on the outer capillary, inhibiting bonding between the glass surface and the PDMS bearing. Figure 1c shows a micrograph time series of fiber extrusion and helix formation upon outer capillary wall rotation (Video S1, Supporting Information).

Twisting of fibers begins near the extrusion nozzles immediately after the rotation has been initiated. After 1 rotation of the outer cylinder the fibers have twisted half a period around the central axis (indicated by arrows). With the second wall rotation completed the fibers have twisted a full period around the central axis. This trend continues with each wall rotation adding another half period. Simultaneously, the fiber bundle becomes tighter indicated by a decreasing pitch length (horizontal length of a full twist): At 1 wall rotation the pitch length is 4.4 mm, at 2 wall rotations 2.0 mm, and at 4 wall rotations it reaches a steady state value of 1.4 mm (see the Supporting Information).

As expected, the rotational speed (revolutions per minutes) controls how tight the bundle is twisted. **Figure 2**ai shows micrographs of steady state bundles at different rpm, constant water flow rate Q_w of 0.8 mL min^{-1} and ternary mixture pressure of 400 kPa (Video S2, Supporting Information). The bundle "tightness" is quantified by the helix angle α as depicted in Figure 2aii. The helix angle α can be determined by measuring the radius of the bundle and the helix pitch (repetition length) from the micrographs (see the Supporting Information). Increasing from 1390 to 3000 rpm results in a linear increase of α from 10° to 27° (Figure 2aii).

Interestingly, the bundle geometry also depends on the water flow rate. Figure 2bi shows micrographs of steady state fiber bundles at different Q_w, constant rpm of 3000 and ternary mixture pressure of 400 kPa (Video S3, Supporting Information). The bundles become progressively tighter with decreasing Q_w. The helix angle α decreases linearly from 37° at 0.5 mL min^{-1} to 18° at 1 mL min^{-1} (Figure 2bii).

3. Discussion

Our results show that the bundle tightness depends on two control parameters: (i) rpm, and (ii) Q_w. This indicates a balance between forces in rotational and in flow direction. In the following, we approximate the forces acting on the fiber bundle based on a hydrodynamic model.

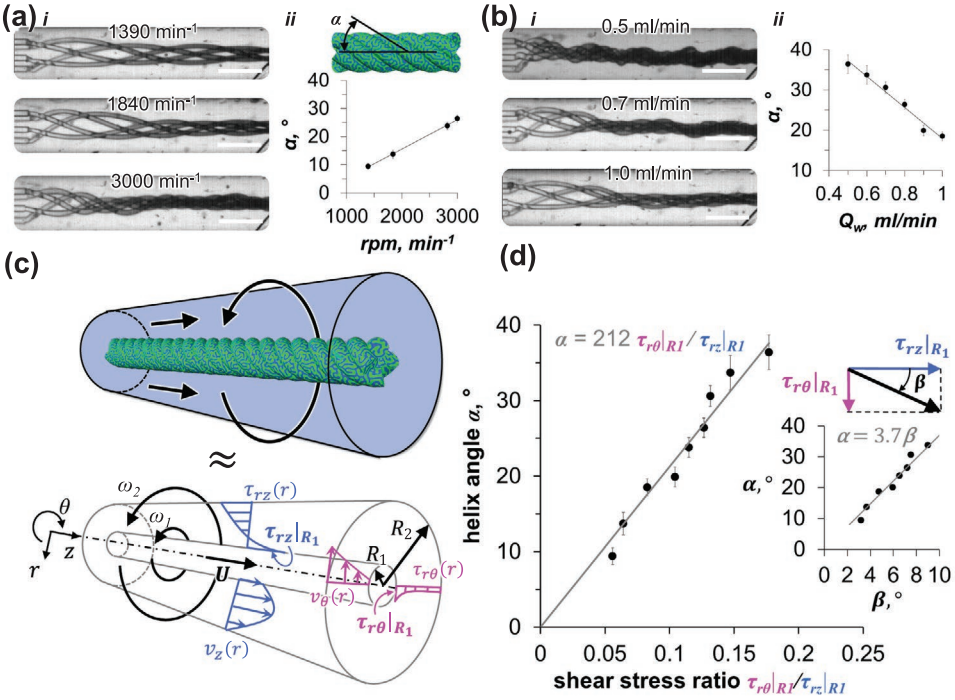

Figure 2. Hydrodynamic study of steady state bundles. ai) Micrographs for different rotational speeds (rpm) at constant water flow rate of 0.8 mL min^{-1}, aii) helix angle measurements. bi) Micrographs for different water flow rates at 3000 rpm, bii) helix angle measurement, all scale bars are 0.5 mm. The lines in the diagrams of (a) and (b) are drawn to guide the eye. c) 3D depiction of bijel bundle in flow channel with arrows indicating flow direction of water and rotation direction of outer wall and cylindrical annulus geometry used to approximate fiber bundle in channel for hydrodynamic calculations. d) Measurements of the helix angle α plotted against calculated values for the shear stress ratio $\tau_{r\theta}|_{R1}/\tau_{rz}|_{R_1}$. Error bars correspond to the standard deviation of 5 measurements. The inset shows a schematic of the angle β and the variation of α with respect to β.

The flow space for the water around the bundle is approximated as a cylindrical annulus (Figure 2c). In this model, the outer wall rotates uniformly with angular velocity ω_2 around the axis of a centered cylinder. The centered cylinder approximates the shape of the bundle, which itself rotates with angular velocity ω_1 and translates with velocity U. The bundle surface velocities U can be determined by measuring the movement of irregularities on the fiber surface via high speed video-microscopy (see the Supporting Information). Two Navier-Stokes Equations (NSE) are solved to calculate velocity ($v_z(r)$, $v_\theta(r)$) and shear stress profiles ($\tau_{rz}(r)$, $\tau_{r\theta}(r)$) around the bundle (see the Supporting Information and Figure 2c). The shear stress ratio $\tau_{r\theta|R_1}/\tau_{rz|R_1}$ is defined to approximate the forces on the bundle surface. In Figure 2d the helix angle α is plotted against $\tau_{r\theta|R_1}/\tau_{rz|R_1}$.

The dependence of α on the shear stress ratio is approximately linear in the studied range and shows the combined effect of the hydrodynamic forces. Interestingly, for all experiments, $\tau_{r\theta|R_1}/\tau_{rz|R_1}$ is always smaller than 0.2, indicating that hydrodynamic forces in axial direction dominate over the rotational shear stresses. When $\tau_{r\theta|R_1}/\tau_{rz|R_1}$ is gradually increased from 0.05 to 0.18, α increases from 10° to 37°.

An alternative representation of the shear stress ratio is given by the angle β, which represents the direction of the resulting vector with the components $\tau_{r\theta|R_1}$ and $\tau_{rz|R_1}$. A plot of α against β is shown in the inset of Figure 2d. The slope of this linear dependence can be interpreted as the resistance of the fibers against twisting, which is likely a function of the fiber bending modulus, as well as the packing constraints in the bundle. However, additional experimental research probing the dependence of the slope on the fiber material properties is needed to develop an analytical prediction.

To probe the impact of inertial forces we calculate the Reynolds numbers for the water around the fibers in rotational (Re_θ) and translational (R_{eZ}) directions (see the Supporting Information). For our experiments with bundles made of 4 fibers Re_θ ranges from 20 – 45, and Re_Z ranges from 10 – 23. The ratio Re_θ/Re_Z increases from 1 to 4 when the helix angle increases from 10 – 38°. These calculations confirm laminar flow in both directions and that inertial effects are larger in rotational direction.

The flow rate of the ternary mixture Q_t is controlled by the pressure. All experiments are performed at a pressure of 400 kPa. For lower pressures periodic fiber pinch-off occurs due to fiber yielding, while for higher pressures nonuniform fiber extrusion takes place.[24] It is possible to increase Q_t and still extrude uniform fibers, but then also Q_w needs to be increased to maintain enough shear stress. However, in order to obtain significant twist angles an increase of Q_w requires an increase of the rpm. The simultaneous increase of Q_t, Q_w, and rpm increases the bundle extrusion speed at a constant bundle size.

At the constant pressure of 400 kPa for the ternary mixture, stable bundles can be obtained within a range of Q_w from 0.5 to 1.0 mL min^{-1}. Outside of this range 3 distinct phenomena are observed: (i) clogging of the extrusion capillary by the solidifying ternary mixture (Q_w < 0.5 mL min^{-1}), (ii) pinch-off of

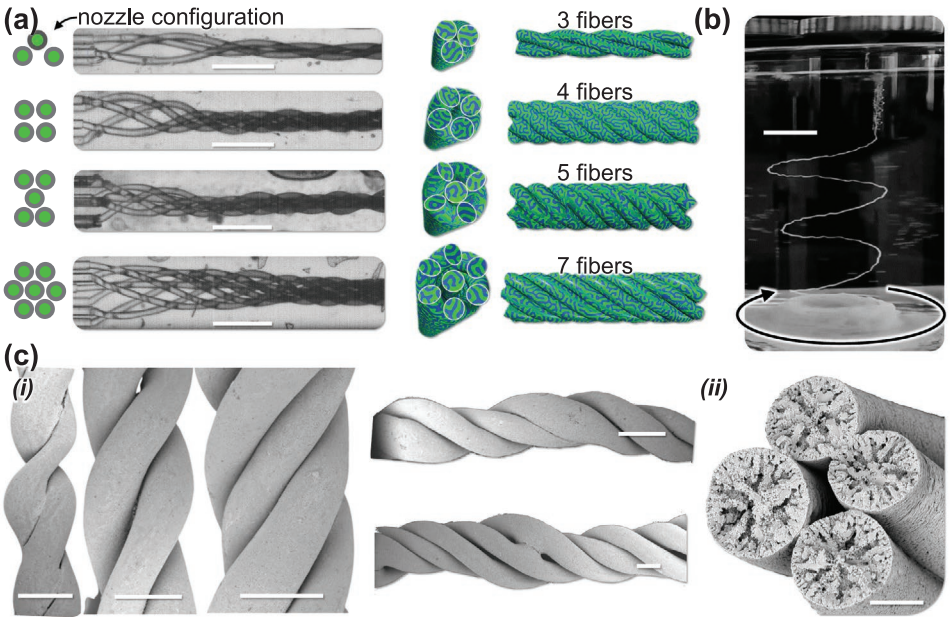

Figure 3. Fabrication of bundles with variable numbers of fibers. a) Left: Schematics showing radial positions for different numbers of extrusion nozzles. Middle: Corresponding micrographs of bundles with 3, 4, 5, and 7 fibers at 3000 rpm and 0.8 mL min^{-1} water flow rate (scale bar: 0.5 mm). Right: 3D schematics of cross-sectional and side views of fiber bundles with 3, 4, 5, and 7 fibers. b) Photograph of a bundle exiting the microfluidic device into a rotating water filled vial (scale bar: 1 cm). c) Scanning electron microscopy, i): Side views of bundles with 2, 3, and 4 fibers (scale bar: 0.1 mm). ii): Cross sectional view of a bundle (scale bar: 0.05 mm).

individual fibers ($Q_w > 1$ mL min^{-1}), (iii) loose bundle formation for low rpm values. Figure SI22 in the Supporting Information depicts these operational limits graphically.

The control over hydrodynamic forces allows for the formation of bundles with defined geometries. In the following, we introduce material applications based on extending the bundle geometry and features.

Up to 7 fibers can be twisted into a single bundle with the capillary combinations employed here. To this end, a desired number of extrusion capillaries (50 µm nozzle diameter) are positioned within the outer tube (0.8 mm inner diameter, see the Supporting Information for details of assembly). **Figure 3**a illustrates the nozzle configuration and twisting process of bundles made with 3, 4, 5, and 7 fibers (Video S4, Supporting Information).

The nozzle positioning controls the bundle organization. With 3 and 4 nozzles, extrusion takes place at the same radial position. As a result, the fibers twist uniformly around each other. However, for 5 and 7 nozzles the fibers are twisted around one central fiber as illustrated in Figure 3a.

Continuous collection of bundles is realized by submerging the outlet of the microfluidic device into a rotating water filled container (Figure 3b). Solid fiber bundles can be obtained after polymerization by UV-light of bijels with acrylic monomers as the oil phase (e.g., butanedioldiacrylate). Scanning electron microscopy shows the bundle geometry and the asymmetric internal fiber structure (Figure 3c).

Feeding the extrusion nozzles with separate liquid casting mixtures enables the formation of composite bijel fiber bundles. We demonstrate this by introducing two fluorescent dyes (Nile Red and Coumarin 6) into different bijel casting mixtures. The polymerized bundles made of fiber strands containing different dyes are visualized with a confocal laser scanning microscope operated in dual channel mode (channel 1: 500–550 nm, channel 2: >630 nm). **Figure 4**a shows confocal laser scanning micrographs of various composite bijel fiber bundles. As noted earlier, bundles formed with 2, 3, and 4 extrusion nozzles contain exclusively twisted fibers. In contrast, with 5 extrusion nozzles the central fiber remains untwisted. This unique architecture enables the formation of high-tensile strength bijel fiber bundles by selective polymerization as shown in the following.

Selective polymerization is carried out while twisting 4 fibers made of diethylphthalate around a central fiber containing monomer and photoinitiator (ethylene glycol dimethacrylate and 2-hydroxy-2-methylpropiophenone). UV-light irradiation polymerizes only the central fiber, while the 4 twisted fibers remain liquid (Figure 4b). Unlike unpolymerized bundles, the polymer/liquid fiber composite can be picked up with tweezers without breaking. We mount this composite in a tensile tester and record the stress vs. strain curve. The original stress-strain curves are non-linear due to straightening of the curved bundle during the experiment. However, after straightening, the bundles elongate linearly. The linear parts of 3 averaged and rescaled stress-extension measurements are shown in Figure 4c (see the Supporting Information for details). An average tensile strength of 20 ± 3.1 MPa is found, which is roughly 4000 times higher than that of the liquid bijel fibers.[28] The average elastic modulus amounts to 1.1 ± 0.4 GPa, reflecting the stiff nature of the highly cross-linked poly(ethylene glycol dimethacrylate).

While the unpolymerized liquid twisted fibers remain fragile, the polymerized central fiber acts as a backbone for

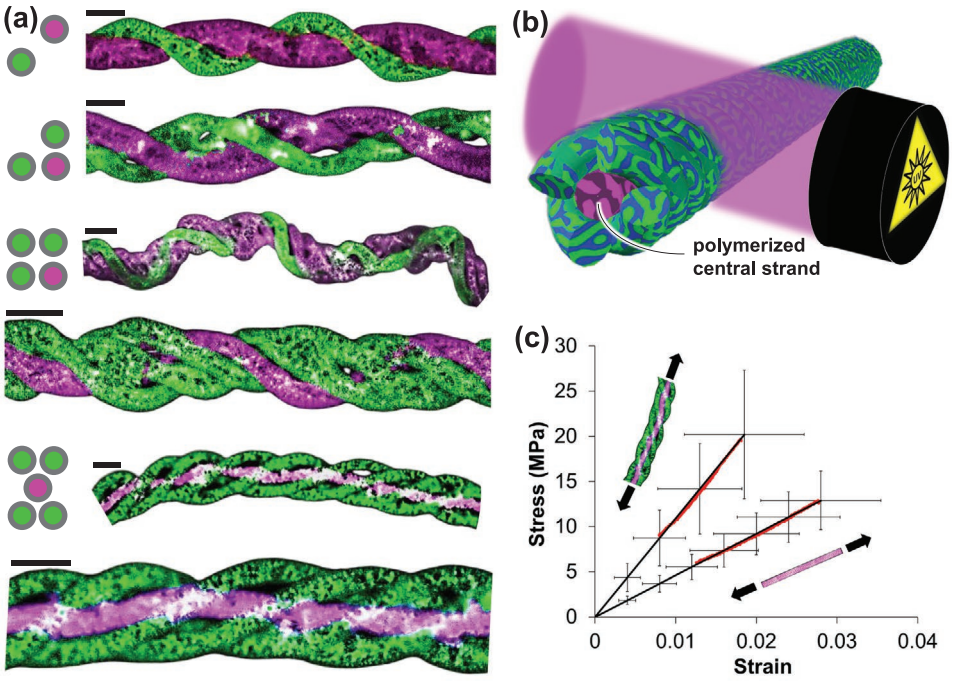

Figure 4. Composite bundles and tensile strength measurement: a) Fluorescence confocal laser scanning micrographs of bundles made of 2, 3, 4 and 5 fibers with fibers colored in magenta dyed with Nile red, and fibers in green dyed with Coumarin 6 (scale bars: 0.1 mm). b) Schematics of selective polymerization of the central fiber in a bundle with 5 fibers. c) Tensile strength measurement of a bundle with 1 central polymerized fiber and 4 unpolymerized twisted fibers (top) and individual polymerized fiber (bottom).

the unpolymerized twisted fibers. Our tensile strength measurement captures only the mechanical strength of the central fiber since the contribution of the twisted fibers to the tensile strength is negligible. Measuring the stress-extension of a single polymerized fiber shows the same magnitude of tensile strength as the composite bundle (13 ± 3 MPa, Figure 4c). The slightly lower tensile strength of the individual fiber is related to differences in the initial ternary mixture used for fiber extrusion, resulting in a lower connectivity of the polymerized domains within the internal structure of the fiber.

During mechanically demanding applications of the composite bijel fiber bundle, the polymerized central fiber will uptake the main load, with minimal mechanical stress and deformation of the 4 twisted liquid bijel fibers. This configuration is advantageous, because it allows to exploit the liquid like properties of the unpolymerized bijel fibers with potentials in fluid transport and biphasic catalysis, while simultaneously providing the high mechanical strengths of a polymeric material.

Our experimental work includes the mechanical tests for a bundle with one centered polymerized fiber and 4 twisted fibers at a fixed helix angle α of 42°. Since the central fiber provides the main mechanical support, changing α or the number of unpolymerized fibers does not significantly affect the tensile strength. The diameter of the central polymerized fiber will change the absolute force needed for breaking, but not the cross-sectional area normalized tensile strength. The main control parameter to change the tensile strength is the composition of the ternary mixture used to generate the central polymerized fiber. The ternary composition affects the interconnectivity of the polymerized domains within the central fiber as shown in our previous study.[18] However, more experimental research is needed to understand the mechanical properties of the composite bundles in dependence of the ternary mixture composition.

4. Conclusion

In conclusion, we have introduced microfluidic in-situ twisting to generate bijel fiber bundles. We demonstrate the control of geometrical features of the bundles based on balancing hydrodynamic stresses in rotational and translational directions. The microfluidic twisting method can produce bundles with pitch lengths from 500 to 2400 µm and helix angles from 10° to 36°. Microscopic bundles at a rate of 5.6 $cm^3\ h^{-1}$ can be produced with our device, but higher rates are possible when increasing feed pressure and rotational speed. Our method is suitable for soft fibers with elastic moduli below 1 MPa and yield strengths ranging from hundreds of Pa to MPa. Microfluidic twisting is applicable to fibers made of bijels, reconfigurable printed liquids,[29] hydrogels,[30] capillary suspensions,[31] high-internal phase emulsions or colloidal gels.[32] Selective polymerization allows for the formation of high-tensile strength composite bundles. In future work, microfluidic twisting can be used to combine fibers with different mechanical properties, chemical compositions and building blocks to generate multi-functional composite bundles with enhanced mechanical, transport, and catalytic properties.

Supporting Information

Supporting Information is available from the Wiley Online Library or from the author.

Acknowledgements

This project has received funding from the European Research Council (ERC) under the European Union's Horizon 2020 research and innovation programme (Grant agreement No. 802636). S.P.K. was supported by NSF career award 1751479.

Conflict of Interest

The authors declare no conflict of interest.

Keywords

bijels, composites, microfluidics, nanoparticles, soft matter

Received: April 23, 2020
Revised: May 9, 2020
Published online: July 6, 2020

[1] Y. Snir, R. D. Kamien, *Science* **2005**, *307*, 1067.
[2] Y. Han, L. Zhao, J. Y. Ying, *Adv. Mater.* **2007**, *19*, 2454.
[3] G. M. Grason, R. F. Bruinsma, *Phys. Rev. Lett.* **2007**, *99*, 098101.
[4] M. S. Turner, R. W. Briehl, F. A. Ferrone, R. Josephs, *Phys. Rev. Lett.* **2003**, *90*, 128103.
[5] J. W. Weisel, C. Nagaswami, L. Makowski, *Proc. Natl. Acad. Sci. USA* **1987**, *84*, 8991.
[6] A. Kuzyk, R. Schreiber, Z. Fan, G. Pardatscher, E. M. Roller, A. Högele, F. C. Simmel, A. O. Govorov, T. Liedl, *Nature* **2012**, *483*, 311.
[7] J. G. Gibbs, A. G. Mark, T. C. Lee, S. Eslami, D. Schamel, P. Fischer, *Nanoscale* **2014**, *6*, 9457.
[8] N. M. Ribe, M. Habibi, D. Bonn, *Annu. Rev. Fluid Mech.* **2012**, *44*, 249.
[9] T. Luelf, C. Bremer, M. Wessling, *J. Memb. Sci.* **2016**, *506*, 86.
[10] C. M. Leech, *The Modelling and Analysis of the Mechanics of Ropes*, Vol. *209*, Springer, Dordrecht **2014**.
[11] H. A. McKenna, J. W. S. Hearle, N. O'Hear, *Handb. Fibre Rope Technol.* **2004**.
[12] J. Zheng, X. Yan, M. M. Li, G. F. Yu, H. Di Zhang, W. Pisula, X. X. He, J. L. Duvail, Y. Z. Long, *Nanoscale Res. Lett.* **2015**, *10*, 475.
[13] L. Q. Liu, M. Eder, I. Burgert, D. Tasis, M. Prato, H. D. Wagner, *Appl. Phys. Lett.* **2007**, *90*, 083108.
[14] C. Zhang, C. Gao, M. W. Chang, Z. Ahmad, J. S. Li, *Appl. Phys. Lett.* **2016**, *109*, 151903.
[15] K. Stratford, R. Adhikari, I. Pagonabarraga, J. C. Desplat, M. E. Cates, *Science* **2005**, *309*, 2198.
[16] E. M. Herzig, K. A. White, A. B. Schofield, W. C. K. Poon, P. S. Clegg, *Nat. Mater.* **2007**, *6*, 966.
[17] J. W. Tavacoli, J. H. J. Thijssen, A. B. Schofield, P. S. Clegg, *Adv. Funct. Mater.* **2011**, *21*, 2020.
[18] M. F. Haase, K. J. Stebe, D. Lee, *Adv. Mater.* **2015**, *27*, 7065.
[19] S. Boakye-Ansah, M. S. Schwenger, M. F. Haase, *Soft Matter* **2019**, *15*, 3379.
[20] M. Pera-Titus, L. Leclercq, J. M. Clacens, F. De Campo, V. Nardello-Rataj, *Angew. Chem., Int. Ed.* **2015**, *54*, 2006.
[21] G. Di Vitantonio, T. Wang, M. F. Haase, K. J. Stebe, D. Lee, *ACS Nano* **2019**, *13*, 26.
[22] S. Cha, H. G. Lim, M. F. Haase, K. J. Stebe, G. Y. Jung, D. Lee, *Sci. Rep.* **2019**, *9*, 6363.
[23] J. A. Witt, D. R. Mumm, A. Mohraz, *J. Mater. Chem. A* **2016**, *4*, 1000.
[24] D. Cai, F. H. Richter, J. H. J. Thijssen, P. G. Bruce, P. S. Clegg, *Mater. Horiz.* **2018**, *5*, 499.
[25] M. F. Haase, H. Jeon, N. Hough, J. H. Kim, K. J. Stebe, D. Lee, *Nat. Commun.* **2017**, *8*, 1234.
[26] T. J. Thorson, E. L. Botvinick, A. Mohraz, *ACS Biomater. Sci. Eng.* **2018**, *4*, 587.
[27] H. Firoozmand, D. Rousseau, *Food Hydrocoll.* **2015**, *48*, 208.
[28] M. F. Haase, N. Sharifi-Mood, D. Lee, K. J. Stebe, *ACS Nano* **2016**, *10*, 6338.
[29] J. Forth, X. Liu, J. Hasnain, A. Toor, K. Miszta, S. Shi, P. L. Geissler, T. Emrick, B. A. Helms, T. P. Russell, *Adv. Mater.* **2018**, *30*, 1707603.
[30] M. A. Daniele, S. H. North, J. Naciri, P. B. Howell, S. H. Foulger, F. S. Ligler, A. A. Adams, *Adv. Funct. Mater.* **2013**, *23*, 697.
[31] E. Koos, *Curr. Opin. Colloid Interface Sci.* **2014**, *19*, 575.
[32] R. V. Bell, C. C. Parkins, R. A. Young, C. M. Preuss, M. M. Stevens, S. A. F. Bon, *J. Mater. Chem. A* **2016**, *4*, 813.